THE JOURNAL OF PHYSICAL CHEMISTRY C

Article

pubs.acs.org/JPCC

Minimization of Ionic Transport Resistance in Porous Monoliths for Application in Integrated Solar Water Splitting Devices

Tom Bosserez,[†] Lisa Geerts,[†] Jan Rongé,*[,†] Frederik Ceyssens,[‡] Sophia Haussener,[§] Robert Puers,[‡] and Johan A. Martens[†]

[†]Centre for Surface Chemistry and Catalysis, KU Leuven, Celestijnenlaan 200F, B-3001 Heverlee, Belgium

[‡]ESAT-MICAS, KU Leuven, Kasteelpark Arenberg 10, B-3001 Heverlee, Belgium

[§]Laboratory of Renewable Energy Science and Engineering, École Polytechnique Fédérale de Lausanne (EPFL), Station 9, 1015 Lausanne, Switzerland

Supporting Information

ABSTRACT: Monolithic solar water splitting devices consist of photovoltaic materials integrated with electrocatalysts and produce solar hydrogen by water splitting upon solar illumination in one device. Upscaling of monolithic solar water splitting devices is obstructed by high ohmic losses in the electrolyte due to long ionic transport distances. A new design overcomes the problem by introducing micron sized pores in a silicon wafer substrate coated with electrocatalysts. A porous solar hydrogen device was simulated by applying a current corresponding to ca. 10% solar-to-hydrogen efficiency. Porous monoliths of 550 μm thickness with varying pore size and spacing were fabricated by laser ablation and electrochemically characterized. Ohmic losses well below 100 mV were reached at 14.4% porosity with 77 μm pores spaced 250 μm apart in 0.25 M KOH electrolyte. In 1 M KOH, 100 mV was reached at 6% porosity with 1 mm pore spacing. Our results suggest ohmic losses below 50 mV can be achieved when using 10 μm thick substrates at 0.2% porosity. These findings make it possible for monolithic solar water splitting devices to be scaled without loss of efficiency.

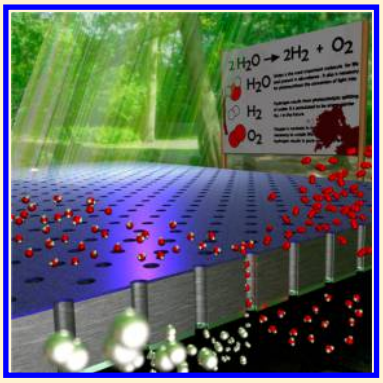

INTRODUCTION

Hydrogen is one of the promising energy vectors that will likely be part of the future sustainable energy portfolio.[1] Using sunlight to split water into hydrogen and oxygen is a viable option for solar hydrogen production and several technologies exist that achieve water splitting at high efficiency.[2] A direct way to produce solar hydrogen is by using a solar water splitting device which combines light absorption, charge separation and electrochemical reactions in an integrated device.[3] High solar-to-hydrogen (STH) efficiencies are reached using high-end photovoltaics (PV) coupled to electrocatalysts submerged in concentrated aqueous electrolyte.[4−7] The use of robust earth-abundant catalysts and stable light absorbing materials with suitable band gaps has also been demonstrated.[8−11] These approaches show great promise at lab scale and development of practical systems is ongoing.[12−16] Beside the performance of catalysts and light absorbers, cell design is important and ohmic losses need to be minimized to maximize overall efficiency.[17,18] There are two common design types.[19,20] In the "wired" design (Figure 1A) planar anode and cathode have opposed surfaces at close proximity such that the interelectrode distance to be covered by ions in the liquid electrolyte is minimized.[9−11]

The "wireless" or "monolithic" layout (Figure 1B) simplifies cell design by eliminating electrical contacts and wires through integration of all components in a monolithic flat assembly.[10]

These two designs differ in the way ionic transport is organized.[19] The overall transport distance between electrodes dictates the ohmic losses of the ions in the electrolyte and can contribute significantly to the overall operating voltage.[19,21] Ohmic losses are often minimized by using concentrated acid or alkaline electrolytes such as H_2SO_4, $HClO_4$, or KOH at concentrations of 0.5 M or higher.[4,5,14,22,23] In wireless systems with flat monoliths consisting of dense PV and electrocatalysts mounted on either side, ions need to travel around the dense monolith to cover the distance between anode and cathode. Already at the centimeter scale unacceptable ohmic losses of hundreds of millivolts and more are to be expected.[19,21]

A straightforward way to achieve anode−cathode proximity in a flat monolithic system is by providing ionic shortcuts. Recently an innovative concept was reported that efficiently achieves low ionic transport distances and low ohmic losses in a monolithic assembly by Si microwires into an electrical and ionic conducting membrane.[24] This concept suffers from complicated manufacturing procedures and generates low photovoltage, which can be alleviated by the application of passivation strategies.[25,26] In this work, we propose another way of achieving short ion transport distances, namely by

Received: July 6, 2016
Revised: August 16, 2016

DOI: 10.1021/acs.jpcc.6b06766
J. Phys. Chem. C XXXX, XXX, XXX−XXX

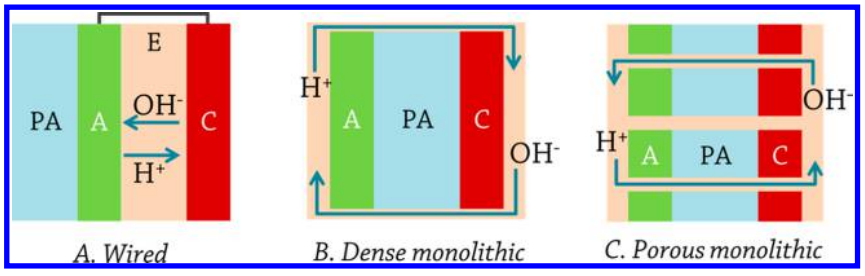

Figure 1. Design types of solar water splitting devices and indication of acid (H^+) or alkaline (OH^-) ion transport pathways. A = anode, C = cathode, PA = photoabsorber, and E = electrolyte.

Table 1. Properties of Porous Monolithic Samples

Sample	A	B	C	D
Pore diameter at anode side [μm]	77	232	1340	4600
Pore diameter at cathode side [μm]	135	316	1340	4600
Pore spacing [mm]	0.25	1	5	17.7
Number of pores	5030	316	12	1
Porosity [%]	14.4	6.0	5.3	5.3
Pore configuration	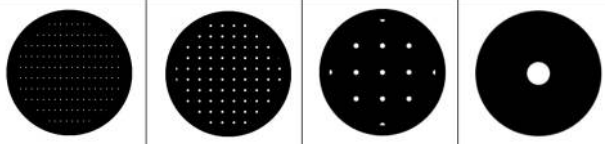			

perforation of monolithic assemblies (Figure 1C). Systematic perforation could be applied to monoliths whatever their size. Additionally such design can easily achieve product separation by introducing a membrane, avoiding dangerous mixing of hydrogen and oxygen and requiring low membrane quantities, depending on the porosity.

We have investigated the ionic transport aspects of the new design type by using an oxidized silicon wafer, coated with electrocatalysts and perforated using laser ablation. Different pore designs and their influence on the ohmic losses of the device were studied. By application of a current across anode and cathode (without illumination), a porous monolithic solar water splitting device with ca. 10% STH efficiency was simulated. Minimization of ohmic losses well below 100 mV in KOH electrolyte is demonstrated. Guidelines for optimum pore configuration are provided.

EXPERIMENTAL SECTION

Preparation of Porous Monolithic Assemblies. N-type silicon wafers (Cemat Silicon, 4″ unpolished, 3−10 ohm cm) with a thickness of 525−575 μm were used as substrate for porous monoliths. RCA cleaning was followed by wet oxidation at 1100 °C for 2 h to obtain an insulating layer of SiO_2 on both sides of the wafer. Thin catalyst films were sputtered on the wafer using Balzers BAE 370 sputtering tool. First, a Ti/W ($Ti_{10}W_{90}$ target, 99.95%) adhesion layer was sputtered at 2.10^{-3} mbar Ar and 150 W for 1 min on both sides. Then, for the cathode, Pt (Pt target, 99.95%) was sputtered at 100 W for 3 min, other parameters unchanged. The anode was sputtered with Ir (Ir target, 99.9%) under Ar atmosphere at 200 W for 5 min. Subsequently an IrO_x layer was sputtered under Ar/O_2 (10:1 volume ratio) at 200 W for 2 min. As deposited anode and cathode catalyst layers measured 400 and 120 nm in thickness, respectively. Pores were introduced in the as prepared wafers by laser ablation (HDYAG, 1064 nm, spot size ca. 65 μm). A porosity of 5.3% for all samples was targeted by adjusting the pore radius at preset pore spacing (center to center) (Table 1). Actual pore diameter deviated from targeted diameter at small dimensions. This resulted in a porosity substantially exceeding the aimed value for sample A and B (Table 1). The pores in sample A and B were narrower at the anode side compared to the cathode side. The design of monolith A is schematically represented in Figure 2. Activation of IrO_x to $Ir^{IV}O_2$ thin film was achieved by repetitive cycling from 0 to 1.46 V vs. RHE in 0.5 M H_2SO_4 solution (Figure S3, Supporting Information).

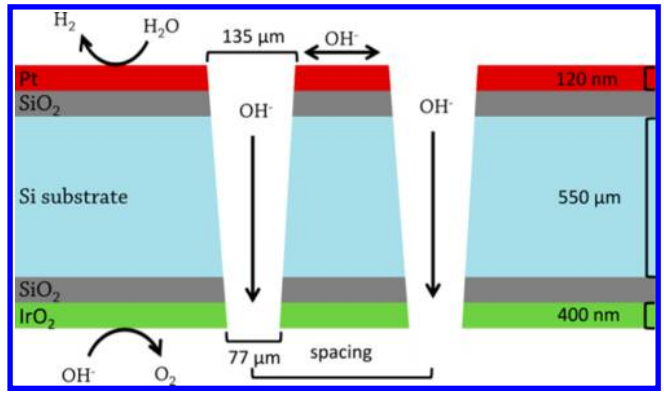

Figure 2. Schematic of porous monolith A.

DOI: 10.1021/acs.jpcc.6b06766
J. Phys. Chem. C XXXX, XXX, XXX−XXX

Electrochemical Characterization of Monolithic Assemblies. Electrochemical characterization was done in an H-type electrochemical cell in two- or three-electrode setup (Figure S4). Experiments were performed in KOH electrolyte with increasing concentration (0.0625, 0.25, and 1 M) and corresponding decreasing resistivity of (73.5 Ω cm, 18.4 Ω cm and 5.6 Ω cm) measured with a calibrated conductivity measuring tool (Tetracon, VWR). Chronopotentiometric (CP) measurement were performed at an applied current density of 7.84 mA cm^{-2}. This corresponds to an STH efficiency of ca. 10% (assuming 100% Faradaic efficiency). Galvanostatic electrochemical impedance spectroscopy (EIS) measurements were performed in 0.0625 M KOH at 1 mA in the frequency range from 1 MHz to 100 Hz in a 2-electrode setup.

Non Ohmic Losses. CP measurements of anode and cathode were performed in a 3-electrode setup. For OER and HER determination, O_2 and H_2 was purged through the respective compartment at 20 mL min^{-1}. The solution was not stirred during measurement. Ag/AgCl (3 M KCl) electrode served as the reference and a Pt ring as the counter electrode. CP measurements were carried out for 60 s and corrected for uncompensated *iR* losses.

Ohmic Losses. CP measurements of the porous monolith were performed in a 2-electrode setup. To avoid transient contributions of concentration polarization by the reaction products, purging of O_2 in the anode compartment and H_2 in the cathode compartment was done to saturate the compartments prior to measurement. The solution was not stirred during measurement. Ohmic losses were obtained by subtracting average kinetic and mass transport losses of both catalysts from the total operating overpotential (Supporting Information). The linear correlation between ohmic losses and resistivity was used to calculate the cell constant. Ohmic loss for sample A in 1 M KOH was below the detection limit via CP measurement (Supporting Information) and was obtained by linear extrapolation.

Product Measurement and Crossover. Product analysis was done by mass spectrometry (Quantitative Gas Analyzer, Hiden Analytical, Warrington, U.K.) with N_2 and Ar as carrier gas at a fixed flow rate (50 mL min^{-1}) in anode and cathode compartment, respectively. Calibration was done using the carrier gas signal. Faradaic efficiency and crossover were calculated from the measured O_2 and H_2 formation rates.

RESULTS AND DISCUSSION

The problem of ohmic losses in integrated solar water splitting devices due to long ionic transport distances is revealed by a simple calculation. Consider a typical wired device (Figure 1A) operating at a current density of 10 mA cm^{-2} in 0.5 M H_2SO_4 electrolyte at 25 °C, (conductivity of 211 mS cm^{-1}) and with anode and cathode separated by 1 cm. The ohmic loss corresponds to 47 mV. Even for such a favorable position of electrodes in close proximity, the ionic transport resistance is of the order of magnitude of a typical kinetic overpotential at a platinum hydrogen evolving electrode.[27] With wireless setups, the ohmic losses are even larger. To illustrate this, a dense square monolith measuring 2.5 × 2.5 cm was immersed vertically in KOH electrolyte solution leaving 0.5 cm of space above and below. Ohmic losses were significant and amounted to 70, 195, and 771 mV in 1.0, 0.25, and 0.0625 M KOH solution, respectively. For the case of 1 M KOH, the ohmic losses already amounted to 15% of the total device overpotential. It illustrates the use of dense submerged monolithic assemblies is no option for designing a scalable and efficient solar water splitting device, in which large ohmic losses cannot be tolerated.[21] The combination of highly active catalysts with a state-of-the-art triple junction solar cell is able to reach 10% STH efficiency if ohmic losses are kept below 100 mV. Therefore, 100 mV is assumed as an upper target in this work (see Supporting Information).

Porous monolithic silicon wafers, coated with electrocatalysts were fabricated and tested for their ohmic losses in a water splitting experiment in alkaline electrolyte. Figure 3 shows the different pore designs that were tested (details in the Experimental Section). A constant porosity for all samples was targeted.

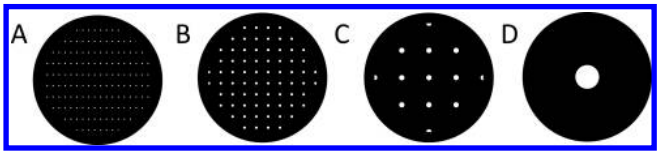

Figure 3. Schematic of the porous monolithic samples A–D with increasing pore size and spacing between pores (pores not to scale). Detailed information can be found in the Experimental Section and in the Supporting Information.

Ohmic losses during water splitting obtained from the perforated monoliths A–D are given in Table 2. The lowest ohmic losses were recorded on monolith A, having the smallest pores and highest porosity. Sample A exhibits ohmic losses below 100 mV in 1 M KOH as well as 0.25 M KOH solution. Monolith B having wider pores and lower porosity achieves the targeted ohmic loss at 1 M KOH. The 1.3 mm size pores in sample C and the single pore measuring 4.6 mm in sample D representing 5.3% porosity are insufficient to reduce ohmic losses to the desired value. Samples C and D show ohmic losses which exceed kinetic overpotentials in a typical solar water splitting device.[21] For each monolith ohmic losses decrease with increasing electrolyte concentration, which is to be expected from Ohm's law.

Table 2. Overview of Ohmic Losses (in mV) Depending on Electrolyte Concentration and Cell Constants K_{cell} [cm^{-1}] for Perforated Monoliths

ohmic losses	sample A	sample B	sample C	sample D
spacing [mm]	0.25	1	5	17.7
0.0625 M KOH	234	648	1471	2928
0.25 M KOH	78	159	347	823
1 M KOH	19	54	145	346
K_{cell} [cm^{-1}]	0.13	0.36	0.83	1.64

Ohmic losses are plotted against pore spacing in Figure 4. For the three investigated KOH concentrations, the ohmic losses increase with increasing pore spacing, highlighting the dominant role of this parameter. Larger pore spacing results in longer transport distances for ions between both electrodes. For samples C and D in 1 M KOH, the ohmic losses are 145 and 346 mV respectively, amounting to more than 30% and 50% of the total required overpotential of the device, showing the dominant effect of large ionic transport distances even at high concentrations. Accepting 100 mV ohmic losses, maximally 1 mm spacing of pores is allowed when operating in 1 M KOH. In 0.25 M solution, the spacing needs to be limited to 250 μm. At these small ionic transport distances,

DOI: 10.1021/acs.jpcc.6b06766
J. Phys. Chem. C XXXX, XXX, XXX–XXX

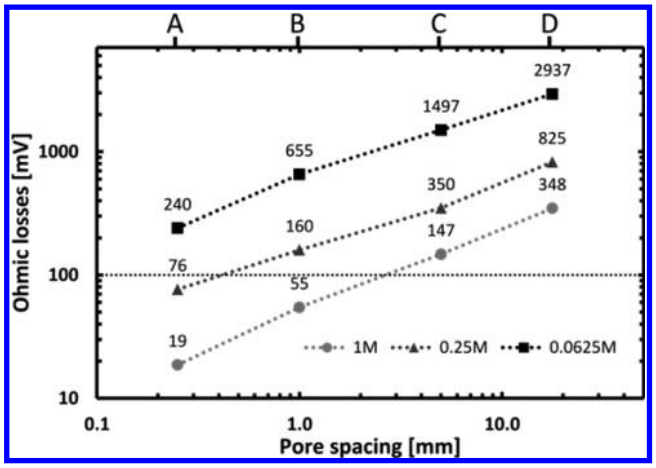

Figure 4. Ohmic losses at applied current density of 7.84 mA cm^{-2}. against pore spacing of samples A, B, C, and D. Concentration values of KOH electrolyte are indicated. In practical solar water splitting devices, ohmic losses below 100 mV are targeted.

ohmic losses only contribute 5% to the total overpotential of the device.

Faradaic efficiencies for hydrogen were over 97% in all instances. Back reaction is expected to be minimal as hydrogen oxidation reaction is poor on the IrO_2 surface.[28] This was evidenced by the lack of a hydrogen adsorption peak in the cyclovoltammetric activation of IrO_x to $Ir^{IV}O_2$ (Supporting Information).

Over 15% of the produced hydrogen was present in the anode compartment, revealing significant transport through the pores from cathode to anode compartment (Figure 5).

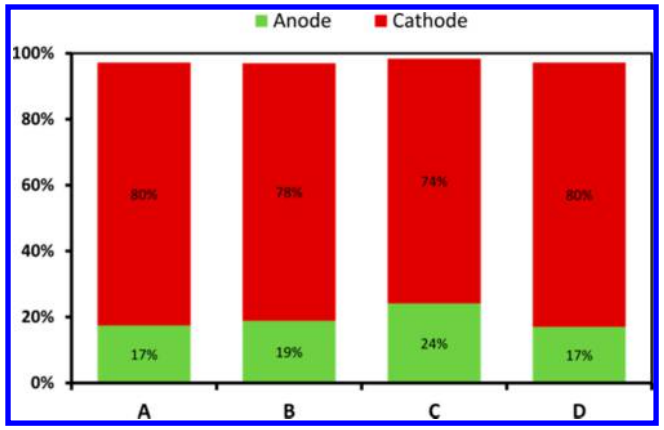

Figure 5. Hydrogen collection yields in cathode and anode compartment. Experimental conditions: 1 M KOH, 25 °C, ca. 10% simulated STH efficiency, collection during continuous operation for 1h and averaged over 7 collection periods.

Hydrogen crossover was little dependent on pore size. In a functional solar water splitting device with porous monolith the pores need to be filled with molecular barrier material to prevent crossover of gaseous products.

In an electrochemical circuit representing the perforated monoliths (Figure 6), the operating potential (ΔE) is a sum of the thermodynamic equilibrium potential (E^0) and any overpotential resulting from the resistances in the circuit (IR_{cell}) at a given current. The main contributions are kinetic overpotential ($IR_{kinetic}$), concentration overpotential (IR_{conc}) and ohmic losses caused by ion transport (IR_{ohmic}). Note that kinetic and concentration overpotentials are not linear and thus do not follow Ohm's law. Other losses such as metallic film resistance (R_{met}) and bubble formation (IR_{rest}) may contribute as well.

$$\Delta E = E^0 + IR_{cell} \quad (1)$$

$$R_{cell} = R_{kinetic} + R_{ohmic} + R_{cp} + R_{met} + R_{rest} \quad (2)$$

Ohmic losses relate here to the resistance of an ionic current in an electrolyte and this resistance is denoted as

$$R_{ohmic} = \frac{l}{A}\rho = \frac{K}{\rho} \quad (3)$$

where l [cm] is the distance between anode and cathode, A [cm^2], the cross section of the ionic pathway, and ρ [Ω cm], the electrolyte resistivity. The ratio of l over A is defined as the cell constant K_{cell} [cm^{-1}] (Table 2). The cell constants were calculated for all porous monoliths and galvanostatic EIS proved a useful tool to measure this property (Figure S9, Supporting Information). In a porous monolith, the ohmic losses (R_{ohmic}) can be subdivided into a pore (R_{pore}) and a surface ($R_{surface}$) contribution with corresponding cell constants K_{pore} and $K_{surface}$. As both contributions are connected in series, the total ohmic losses can be written as

$$R_{ohmic} = K_{cell}\rho = (K_{pore} + 2K_{surface})\rho \quad (4)$$

$K_{surface}$ is determined by the electrolyte height above the surface, pore spacing and porosity pattern. This value cannot be calculated analytically as the exact pathway of ions from the surface to the pore may occur in different ways. In general, a large pore spacing implies that on average an ion produced on the surface will have to travel a longer distance to reach a pore and will thus give rise to larger ohmic resistance or $K_{surface}$ as is represented in Figure 6.

K_{pore} can be calculated because it is dependent only on pore length l_{pore}, i.e., device thickness, and cross sectional surface area of all pores A_{pore}, i.e., monolith porosity ϕ. Assuming a uniform ionic current density over the pore volume, K_{pore} is obtained from

$$K_{pore} = \frac{l_{pore}}{A_{pore}} \quad (5)$$

Figure 7 depicts the contribution of pore and surface losses to total ohmic losses during water splitting. For large pore spacing (C and D) ohmic losses are dominated by surface losses but this tendency reverses for smaller spacing (A and B). With pores spaced less than 1 mm apart, surface ohmic losses become marginal but pore ohmic losses are still substantial.

These losses can only be mitigated by increasing the porosity or reducing the substrate thickness. For example, a device of 55 μm thickness will exhibit a 10-fold decrease in pore ohmic losses compared to a device with 550 μm thickness. Additionally, less concentrated electrolytes could be used while maintaining low ohmic losses, implying less stringent conditions for photoactive materials and catalysts.

Possible drawbacks of porous monoliths for solar hydrogen are the reduced surface area for light absorption, damage to the photoabsorber, and product crossover. To counter these side effects, advanced fabrication methods, the introduction of molecular barriers, and photon management to maximize light absorption at nanoscale will be needed. The introduction of macropores into photovoltaic devices has already been

DOI: 10.1021/acs.jpcc.6b06766
J. Phys. Chem. C XXXX, XXX, XXX−XXX

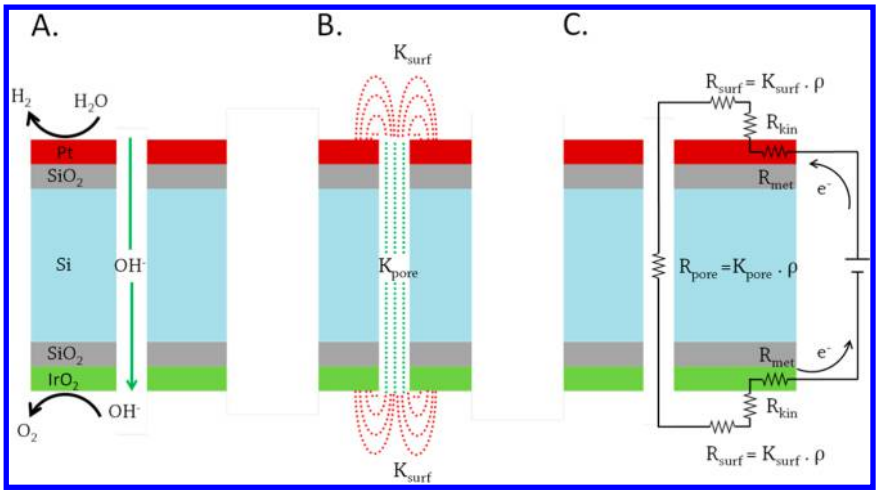

Figure 6. Schematic representation of processes occurring in porous monoliths. (A) General reaction scheme in alkaline conditions. (B) Surface (K_{surf}, red) and pore (K_{pore}, green) ionic pathways in the electrolyte. (C) Equivalent circuit with indication of all resistances.

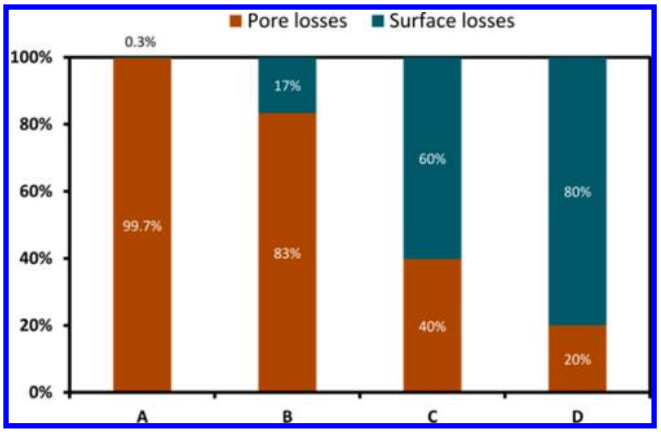

Figure 7. Contribution of pore and surface ohmic losses.

successfully demonstrated by Ernst et al.[29] Carrier lifetimes were enhanced by passivation of pore walls with a thermally grown oxide layer.

CONCLUSIONS

Effective ionic transport management is a key element of the design of efficient, stable and cost-effective monolithic solar water splitting devices. Excessive ohmic losses due to long ion transport distances around flat PV−electrocatalyst assemblies confirm their inherently nonscalable nature. Perforating the monolithic assembly provides short ionic transport pathways and reduces ohmic losses to acceptable levels. Such porous monoliths were fabricated by laser ablation of oxidized silicon wafer coated with electrocatalysts. At a simulated STH efficiency of ca. 10% and using KOH electrolyte, the ohmic losses are easily kept below 100 mV, provided a pore spacing of 1 mm or less is respected and 1 or 0.25 M KOH electrolyte is used. Low ohmic losses could even be achieved at reduced electrolyte concentrations which has the additional benefit of lowering the stringent requirement for both catalysts as well as encapsulation materials when working at extreme pH values

At a pore spacing of 1 mm and less, a simple electrochemical circuit model suggests ohmic losses inside the pores start to dominate over surface ohmic losses. At lower device thickness, ohmic losses are expected to decrease further, even at lower porosity. Multiphysics and multiscale models of porous monoliths are needed to gain deeper insight in concentration, current and potential gradients depending on pore architecture. The results presented here show that porous monolithic solar water splitting devices are to be considered a viable option for large scale solar fuel production systems.

ASSOCIATED CONTENT

Supporting Information

The Supporting Information is available free of charge on the ACS Publications website at DOI: 10.1021/acs.jpcc.6b06766.

Detailed description of sample preparation, OER catalyst activation, electrochemical setup, CP measurements, ohmic losses calculations, galvanostatic EIS, and product crossover measurements (PDF)

AUTHOR INFORMATION

Corresponding Author

*(J.R.) E-mail: Jan.Ronge@biw.kuleuven.be. Telephone: +32 16 32 15 91.

Author Contributions

The manuscript was written through contributions of all authors. All authors have given approval to the final version of the manuscript.

Notes

The authors declare no competing financial interest.

ACKNOWLEDGMENTS

The authors thank Thomas Brockhans for laser ablation and Christine Kirschhock for design of graphical abstract. This work was supported by the Hercules Foundation for heavy equipment (AKUL 034 and ZW1115), by the Flemish Government through long-term structural funding of JAM (Methusalem funding), by the European Research Council under the European Union's Seventh Framework Programme (FP7/2007-2013)/ERC Grant Agreement No. 340931 and by the Starting Grant of the Swiss National Science Foundation as part of the SCOUTS project (Grant No. 155876). J.R. and F.C. acknowledge the Research Foundation-Flanders (FWO) for a fellowship.

REFERENCES

(1) IEA. *Hydrogen and Fuel Cells*; 2015.

DOI: 10.1021/acs.jpcc.6b06766
J. Phys. Chem. C XXXX, XXX, XXX−XXX

(2) Jacobsson, T. J.; Fjällström, V.; Edoff, M.; Edvinsson, T. Sustainable Solar Hydrogen Production: From Photoelectrochemical Cells to PV-Electrolyzers and Back Again. *Energy Environ. Sci.* **2014**, *7*, 2056.
(3) Nielander, A. C.; Shaner, M. R.; Papadantonakis, K. M.; Francis, S. A.; Lewis, N. S. A Taxonomy for Solar Fuels Generators. *Energy Environ. Sci.* **2015**, *8*, 16−25.
(4) Khaselev, O.; Turner, J. A. A Monolithic Photovoltaic-Photoelectrochemical Device for Hydrogen Production via Water Splitting. *Science* **1998**, *280*, 425−427.
(5) Rocheleau, R. E.; Miller, E. L.; Misra, A. High-Efficiency Photoelectrochemical Hydrogen Production Using Multijunction Amorphous Silicon Photoelectrodes. *Energy Fuels* **1998**, *12*, 3−10.
(6) Licht, S.; Wang, B.; Mukerji, S.; Soga, T.; Umeno, M.; Tributsch, H. Over 18% Solar Energy Conversion to Generation of Hydrogen Fuel; Theory and Experiment for Efficient Solar Water Splitting. *Int. J. Hydrogen Energy* **2001**, *26*, 653−659.
(7) Khaselev, O.; Bansal, A.; Turner, J. High-Efficiency Integrated Multijunction Photovoltaic/electrolysis Systems for Hydrogen Production. *Int. J. Hydrogen Energy* **2001**, *26*, 127−132.
(8) Osterloh, F. E. Inorganic Nanostructures for Photoelectrochemical and Photocatalytic Water Splitting. *Chem. Soc. Rev.* **2013**, *42*, 2294−2320.
(9) Han, L.; Abdi, F. F.; van de Krol, R.; Liu, R.; Huang, Z.; Lewerenz, H.-J.; Dam, B.; Zeman, M.; Smets, A. H. M. Efficient Water-Splitting Device Based on a Bismuth Vanadate Photoanode and Thin-Film Silicon Solar Cells. *ChemSusChem* **2014**, *7*, 2832−2838.
(10) Reece, S. Y.; Hamel, J.; Sung, K.; Jarvi, T.; Esswein, A. J.; Pijpers, J. J. H.; Nocera, D. G. Wireless Solar Water Splitting Using Silicon-Based Semiconductors and Earth-Abundant Catalysts. *Science* **2011**, *334*, 645−648.
(11) Urbain, F.; Smirnov, V.; Becker, J.-P.; Rau, U.; Ziegler, J.; Kaiser, B.; Jaegermann, W.; Finger, F. Application and Modeling of an Integrated Amorphous Silicon Tandem Based Device for Solar Water Splitting. *Sol. Energy Mater. Sol. Cells* **2015**, *140*, 275−280.
(12) Modestino, M. A.; Walczak, K. A.; Berger, A. D.; Evans, C. M.; Haussener, S.; Koval, C.; Newman, J.; Ager, J. W.; Segalman, R. a. Robust Production of Purified H2 in a Stable, Self-Regulating, and Continuously Operating Solar Fuel Generator. *Energy Environ. Sci.* **2014**, *7*, 297−301.
(13) Jin, J.; Walczak, K. A.; Singh, M. R.; Karp, C.; Lewis, N. S.; Xiang, C. An Experimental and Modeling/simulation-Based Evaluation of the Efficiency and Operational Performance Characteristics of an Integrated, Membrane-Free, Neutral pH Solar-Driven Water-Splitting System. *Energy Environ. Sci.* **2014**, *7*, 3371−3380.
(14) Walczak, K. A.; Chen, Y.; Karp, C.; Beeman, J. W.; Shaner, M. R.; Spurgeon, J. M.; Sharp, I. D.; Amashukeli, X.; West, W.; Jin, J.; et al. Modeling, Simulation, and Fabrication of a Fully Integrated, Acid-Stable, Scalable Solar-Driven Water-Splitting System. *ChemSusChem* **2015**, *8*, 544−551.
(15) Singh, M. R.; Papadantonakis, K. M.; Xiang, C.; Lewis, N. S. An Electrochemical Engineering Assessment of the Operational Conditions and Constraints for Solar-Driven Water-Splitting Systems at Near-Neutral pH. *Energy Environ. Sci.* **2015**, *8*, 2760−2767.
(16) Ager, J. W.; Shaner, M. R.; Walczak, K. A.; Sharp, I. D.; Ardo, S. Experimental Demonstrations of Spontaneous, Solar-Driven Photoelectrochemical Water Splitting. *Energy Environ. Sci.* **2015**, *8*, 2811−2824.
(17) Chen, Y.; Hu, S.; Xiang, C.; Lewis, N. S. A Sensitivity Analysis to Assess the Relative Importance of Improvements in Electrocatalysts, Light Absorbers, and System Geometry on the Efficiency of Solar-Fuels Generators. *Energy Environ. Sci.* **2015**, *8*, 876−886.
(18) Modestino, M. A.; Haussener, S. An Integrated Device View on Photo-Electrochemical Solar-Hydrogen Generation. *Annu. Rev. Chem. Biomol. Eng.* **2015**, *6*, 13−34.
(19) Newman, J. Scaling with Ohm's Law; Wired vs. Wireless Photoelectrochemical Cells. *J. Electrochem. Soc.* **2013**, *160*, F309−F311.
(20) Bosserez, T.; Rongé, J.; Van Humbeeck, J.; Haussener, S.; Martens, J. Design of Compact Photoelectrochemical Cells for Water Splitting. *Oil Gas Sci. Technol.* **2015**, *70*, 877−889.
(21) Haussener, S.; Xiang, C.; Spurgeon, J. M.; Ardo, S.; Lewis, N. S.; Weber, A. Z. Modeling, Simulation, and Design Criteria for Photoelectrochemical Water-Splitting Systems. *Energy Environ. Sci.* **2012**, *5*, 9922.
(22) Verlage, E.; Hu, S.; Liu, R.; Jones, R. J. R.; Sun, K.; Xiang, C.; Lewis, N. S.; Atwater, H. A. A Monolithically Integrated, Intrinsically Safe, 10% Efficient, Solar-Driven Water-Splitting System Based on Active, Stable Earth-Abundant Electrocatalysts in Conjunction with Tandem III−V Light Absorbers Protected by Amorphous TiO_2 Films. *Energy Environ. Sci.* **2015**, *8*, 3166−3172.
(23) Lin, G. H.; Kapur, M.; Kainthla, R. C.; Bockris, J. O. One Step Method to Produce Hydrogen by a Triple Stack Amorphous Silicon Solar Cell. *Appl. Phys. Lett.* **1989**, *55*, 386.
(24) Spurgeon, J. M.; Walter, M. G.; Zhou, J.; Kohl, P. a.; Lewis, N. S. Electrical Conductivity, Ionic Conductivity, Optical Absorption, and Gas Separation Properties of Ionically Conductive Polymer Membranes Embedded with Si Microwire Arrays. *Energy Environ. Sci.* **2011**, *4*, 1772−1780.
(25) Xiang, C.; Meng, A. C.; Lewis, N. S. Evaluation and Optimization of Mass Transport of Redox Species in Silicon Microwire-Array Photoelectrodes. *Proc. Natl. Acad. Sci. U. S. A.* **2012**, *109*, 15622−15627.
(26) Shaner, M. R.; Hu, S.; Sun, K.; Lewis, N. S. Stabilization of Si Microwire Arrays for Solar-Driven H2O Oxidation to O2(g) in 1.0 M KOH(aq) Using Conformal Coatings of Amorphous TiO2. *Energy Environ. Sci.* **2015**, *8*, 203−207.
(27) Trasatti, S. Work Function, Electronegativity, and Electrochemical Behaviour of Metals. *J. Electroanal. Chem. Interfacial Electrochem.* **1972**, *39*, 163−184.
(28) Slavcheva, E.; Radev, I.; Topalov, G.; Budevski, E. Sputtered Electrocatalysts for PEM Electrochemical Energy Converters. *Electrochim. Acta* **2007**, *53*, 362−368.
(29) Ernst, M.; Brendel, R.; Ferre, R.; Harder, N.-P. Macroporous Silicon as an Absorber for Thin Heterojunction Solar Cells. *Phys. Status Solidi RRL* **2012**, *6*, 187−189.

DOI: 10.1021/acs.jpcc.6b06766
J. Phys. Chem. C XXXX, XXX, XXX−XXX